Supporting Information

Spatially Resolved Visualization of Long-Lived Charge Carriers in Al-Doped $SrTiO_3$ by the Time-Resolved Microscopy

Kana Matsumoto,[1] Yuki Nakatsukasa,[1] Daisuke Ioka, [2] Zhenhua Pan, [2] Seung Heon Choi,[3] Woon Yong Sohn[3,4] and Kenji Katayama[1*]

1 Department of Applied Chemistry, Chuo University, Tokyo 112-8551, Japan;

2 Department of Applied Chemistry, Graduate School of Engineering, University of Hyogo, Himeji, Hyogo 671-2280, Japan;

3 Department of Chemistry, Chungbuk National University, Cheongju, Chungbuk, Korea

4 Chungbuk National University G-LAMP Project Group, Cheongju, Chungbuk, Korea

*Corresponding authors:

K. Katayama, Phone: +81-3-3817-1913, E-mail: kkata.33g@g.chuo-u.ac.jp

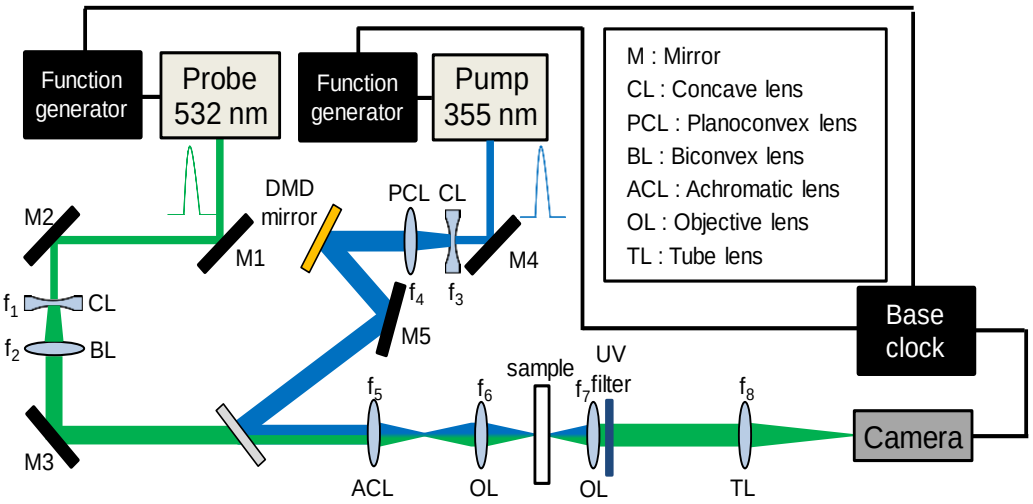

Figure S1 The schematic overview of the optical setup of the patterned-illumination time-resolved phase microscopy (PI-PM) is shown. Pattern illumination was achieved using a digital micromirror device (DMD) (Light Crafter 4500, Texas Instruments). The pump light, reflected off the DMD, created variable light patterns that mirrored those designed on a computer. These patterns were then projected onto the sample, reduced to 1/14th of their original size, through a combination of a lens (f = 100 mm) and an objective lens (LUCPLELN20X, Olympus). The pulsed illumination was synchronized with the pump light via a dichroic mirror and directed onto the sample. The light passing through the sample was captured using another objective lens (LUCPLFLN20x, Olympus) and a tube lens (TTL180-A, Thorlabs), and imaged onto a CMOS camera (MV1-D1024E-160, Photon Focus) with a sensor size of 10.9 x 10.9 mm (1024 x 1024 pixels), focusing on a central strip (200 x 1024 pixels). The diameter of the sample area illuminated by the pump pulse was 0.5 mm. Adjusting the delay between the pump and probe pulses allowed for the capture of a sequence of images, with the temporal resolution being determined by the pulse widths of the pump and probe lights, which ranged from 3 to 5 ns. The pump light was generated by the third harmonic of a Nd:YAG pulse laser (pulse width: 3-5 ns, wavelength: 355 nm) from GAIA, Rayture Systems, while the probe light came from the second harmonic of another Nd:YAG pulse laser (pulse width: 5 ns, wavelength: 532 nm) from the same supplier. The timing of the pulses was meticulously regulated by two function generators (WF1968, NF) synchronized to a base clock (DF1906, NF), each controlling the flash lamp and Q-switch timing with a precision of 100 ps. The intensities of the pump and probe lights were 0.8 mJ/pulse and 0.02 mJ/pulse, respectively.

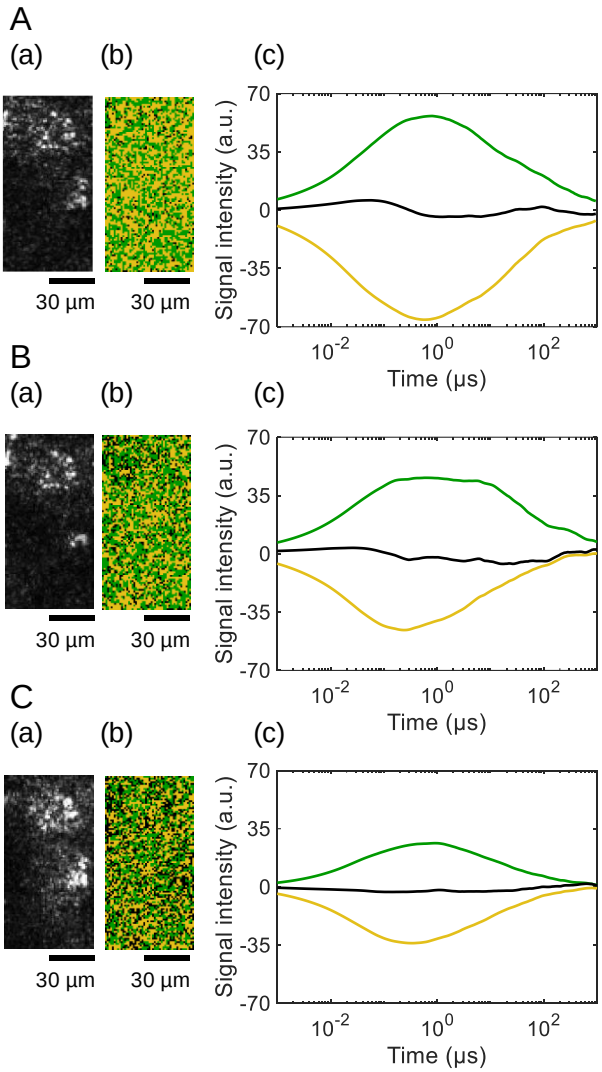

(d)

Solvent	Category	Ratio [%]	Rise [ns]	Decay [µs]
ACN	1 (Green)	42	31 ± 1	23 ± 1
	2 (Yellow)	52	20 ± 1	21 ± 1
	3 (Black)	6	-	-
EtOH	1 (Green)	43	28 ± 1	59 ± 2
	2 (Yellow)	40	18 ± 1	12 ± 1
	3 (Black)	17	-	-
NB/ EtOH	1 (Green)	33	23 ± 1	11 ± 1
	2 (Yellow)	37	19 ± 1	8.4 ± 0.3
	3 (Black)	30	-	-

Figure S2 The clustering analyses of the charge carrier responses of a pristine $SrTiO_3$ in (A) ACN, (B) EtOH, and (C) NB/EtOH in Region 2 in **Figure 1(a)**. (a) correspond to a microscopic image, and the corresponding categorized map is shown in (b), and the scale bar corresponds to 30 µm. The averaged responses for the categorized responses are shown in (c). The area ratios of categories and the rise/decay times for the categories are shown in (d).

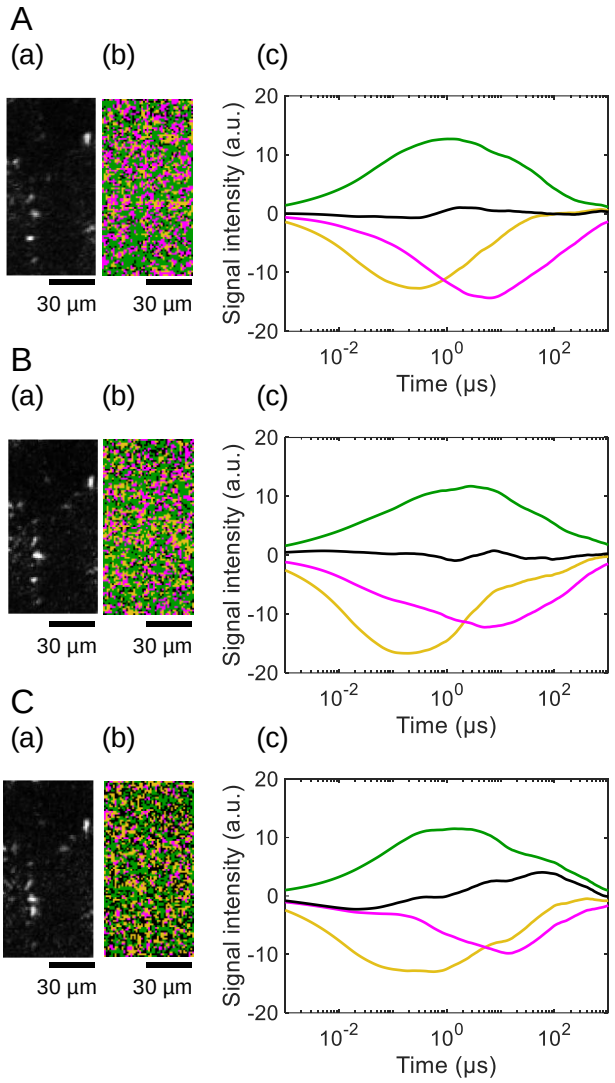

(d)

Solvent	Category	Ratio [%]	Rise [ns]	Decay [μs]
ACN	1 (Green)	47	36 ± 1	42 ± 2
	2 (Yellow)	18	16 ± 1	3.3 ± 0.1
	3 (Black)	10	-	-
	4 (Magenta)	25	247 ± 9	99 ± 4
EtOH	1 (Green)	46	47 ± 2	55 ± 2
	2 (Yellow)	22	12 ± 0	4.7 ± 0.2
	3 (Black)	14	-	-
	4 (Magenta)	18	58 ± 2	144 ± 6
NB/ EtOH	1 (Green)	34	54 ± 2	74 ± 3
	2 (Yellow)	24	12 ± 0	16 ± 3
	3 (Black)	33	-	-
	4 (Magenta)	9	49 ± 2	88 ± 3

Figure S3 The clustering analyses of the charge carrier responses of a Al-doped $SrTiO_3$ ($SrTiO_3$:Al) in (A) ACN, (B) EtOH, and (C) NB/EtOH in Region 1 in **Figure 1(b)**. (a) correspond to a microscopic image, and the corresponding categorized map is shown in (b), and the scale bar corresponds to 30 μm. The averaged responses for the categorized responses are shown in (c). The area ratios of categories and the rise/decay times for the categories are shown in (d).

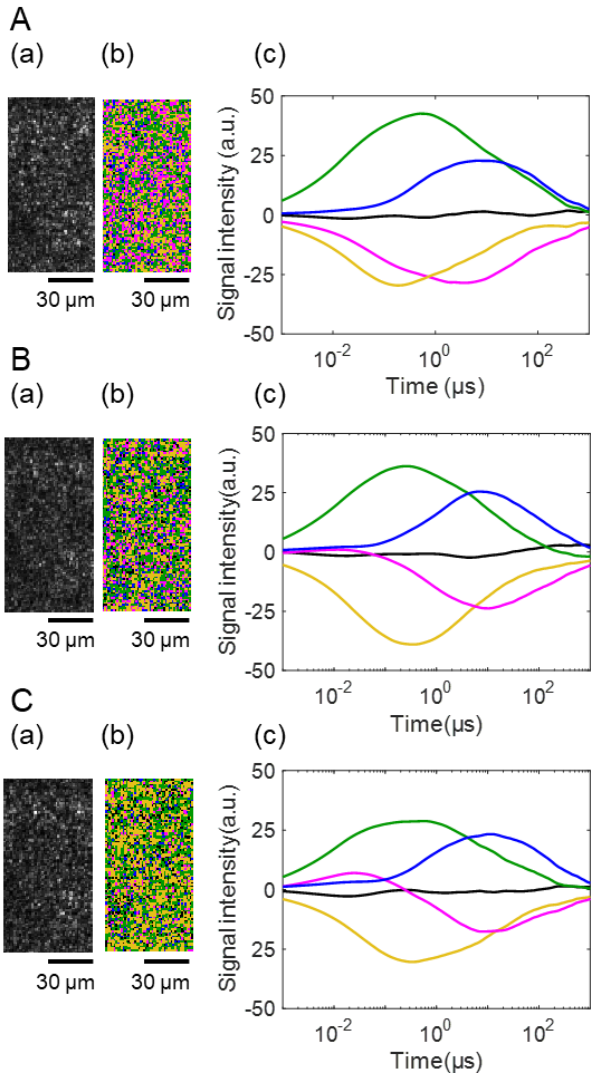

(d)

Solvent	Category	Ratio [%]	Rise [ns]	Decay [μs]
ACN	1 (Green)	35	16 ± 1	15 ± 1
	2 (Yellow)	31	16 ± 1	6.1 ± 0.2
	3 (Black)	3	-	-
	4 (Magenta)	22	55 ± 2	69 ± 3
	5 (Blue)	9	364 ± 13	153 ± 6
EtOH	1 (Green)	37	12 ± 1	7.2 ± 0.3
	2 (Yellow)	31	18 ± 1	6.4 ± 0.2
	3 (Black)	8	-	-
	4 (Magenta)	14	621 ± 23	220 ± 8
	5 (Blue)	10	636 ± 24	116 ± 4
NB/ EtOH	1 (Green)	36	9.8 ± 0.4	10 ± 1
	2 (Yellow)	40	22 ± 1	16 ± 1
	3 (Black)	12	-	-
	4 (Magenta)	6	1095 ± 40	279 ± 10
	5 (Blue)	6	566 ± 21	167 ± 7

Figure S4 The clustering analyses of the charge carrier responses of a Rh/$SrTiO_3$:Al film in (A) ACN, (B) EtOH, and (C) NB/EtOH in Region 1 in **Figure 1(c)**. (a) correspond to a microscopic image, and the corresponding categorized map is shown in (b), and the scale bar corresponds to 30 μm. The averaged responses for the categorized responses are shown in (c). The area ratios of categories and the rise/decay times for the categories are shown in (d).

Simulation Procedure for Charge Carrier Kinetics

To clarify the mechanistic origin of the charge-carrier responses observed by PI-PM, numerical simulations of the transient carrier populations were conducted for $SrTiO_3$, $SrTiO_3$:Al, and Rh/$SrTiO_3$:Al. The simulation framework is shown in Figure S5 and describes the temporal evolution of mobile electrons and holes in the conduction and valence bands (n_m and p_m), together with trapped carriers at surface or defect levels ($n_t(t)$, $p_t(t)$). Mobile carriers are generated immediately after the pump excitation and decay via band-to-band recombination, trapping to defect states, or regenerated via detrapping back into the bands from trap states. Trapped carriers evolve through trapping and detrapping processes governed by rate constants (k_t, k_d), which are linked by a Boltzmann relationship determined by the trap-depth energy. (1,2) The balance between mobile and trapped populations reproduces the refractive-index-derived PI-PM signal, because the observed phase contrast predominantly originates from carriers localized in trap states, whose rise and decay occur on tens–hundreds of nanoseconds timescales.

(1) Nandal, Vikas, Ryota Shoji, Hiroyuki Matsuzaki, et al. "Unveiling Charge Dynamics of Visible Light Absorbing Oxysulfide for Efficient Overall Water Splitting." *Nature Communications* 12, no. 1 (2021): 7055. https://doi.org/10.1038/s41467-021-27199-3.

(2) Chugenji, Tatsuya, Zhenhua Pan, Vikas Nandal, Kazuhiko Seki, Kazunari Domen, and Kenji Katayama. "Local Charge Carrier Dynamics of a Particulate Ga-Doped La5Ti2Cu0.9Ag0.1O7S5 Photocatalyst and the Impact of Rh Cocatalysts." *Physical Chemistry Chemical Physics* 24, no. 29 (2022): 17485–95. https://doi.org/10.1039/D2CP02808E.

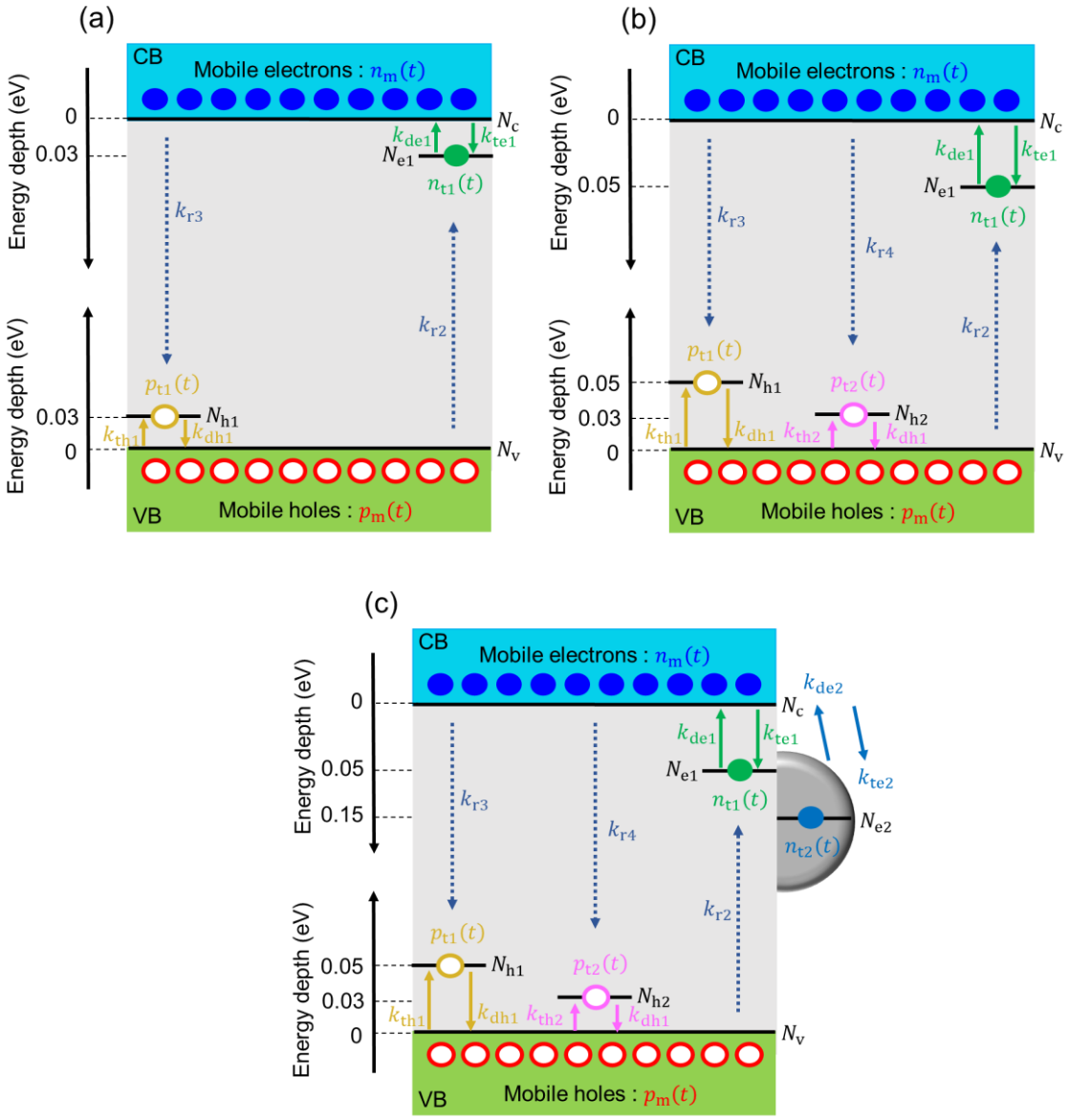

Figure S5 Kinetic simulation model for (a) pristine $SrTiO_3$, (b) $SrTiO_3$:Al, and (c) Rh-doped $SrTiO_3$:Al, and the electron and hole shallow states are assumed, and the corresponding recombination channels are displayed.

For pristine $SrTiO_3$, one electron trap and one hole trap were introduced. The number of the free electrons decreases due to the trapping to the trap state, which is proportional to the trap rate and the available open states at the trap states, $N_{e1} - n_{t1}(t)$, (N_{e1} : surface state density) and also they increase via the detrapping from the trap state, which is proportional to the detrapping rate and the available open state at the conduction states, $N_c - n_m(t)$ (N_c : number of states at the conduction

band) and it follows:

$$\frac{\mathrm{d}n_{\mathrm{m}}(t)}{\mathrm{d}t} = -k_{\mathrm{te1}}\big(N_{\mathrm{e1}} - n_{\mathrm{t1}}(t)\big)n_{\mathrm{m}}(t) + k_{\mathrm{de1}}\big(N_{\mathrm{c}} - n_{\mathrm{m}}(t)\big)n_{\mathrm{t1}}(t) \quad (1)$$

The number of the trapped electrons increases as the above-mentioned trapping process of the free electrons and decreases as the above-mentioned detrapping process, and at the same time, it reduces their number via the recombination with free holes, and it follows:

$$\frac{\mathrm{d}n_{\mathrm{t1}}(t)}{\mathrm{d}t} = k_{\mathrm{te1}}\big(N_{\mathrm{e1}} - n_{\mathrm{t1}}(t)\big)n_{\mathrm{m}}(t) - k_{\mathrm{de1}}\big(N_{\mathrm{c}} - n_{\mathrm{m}}(t)\big)n_{\mathrm{t1}}(t) - k_{\mathrm{r2}}n_{\mathrm{t1}}(t)p_{\mathrm{m}}(t) \quad (2)$$

Similarly, the number of the trap holes increases due to the trapping process of the free holes and decreases due to the detrapping process, and it also decays due to the recombination with free electrons, and it follows:

$$\frac{\mathrm{d}p_{\mathrm{t1}}(t)}{\mathrm{d}t} = k_{\mathrm{th1}}\big(N_{\mathrm{h1}} - p_{\mathrm{t1}}(t)\big)p_{\mathrm{m}}(t) - k_{\mathrm{de1}}\big(N_{\mathrm{v}} - p_{\mathrm{m}}(t)\big)p_{\mathrm{t1}}(t) + k_{\mathrm{r3}}p_{\mathrm{t1}}(t)n_{\mathrm{m}}(t) \quad (3)$$

Since the charge balance should be maintained during the calculation, the number of the mobile holes is calculated from the charge balance as:

$$\frac{\mathrm{d}p_{\mathrm{m}}(t)}{\mathrm{d}t} = \frac{\mathrm{d}n_{\mathrm{m}}(t)}{\mathrm{d}t} + \frac{\mathrm{d}n_{\mathrm{t1}}(t)}{\mathrm{d}t} - \frac{\mathrm{d}p_{\mathrm{t1}}(t)}{\mathrm{d}t} \quad (4)$$

where k_{te1} and k_{th1} are trapping rate constants, k_{de1} and k_{dh1} are detrapping rate constants, and k_{r2} and k_{r3} describe recombination between free and trapped carriers. The detrapping and trapping constants were related through the Boltzmann factor:

$$k_{\mathrm{de}} = k_{\mathrm{te}} \exp\left(-\frac{E_{\mathrm{te}}}{k_{\mathrm{B}}T}\right) \quad (5)$$

$$k_{\mathrm{dh}} = k_{\mathrm{th}} \exp\left(-\frac{E_{\mathrm{th}}}{k_{\mathrm{B}}T}\right) \quad (6)$$

was imposed to satisfy thermal equilibrium, with E_{te} and E_{th} as the trap depths. The density of states of the conduction and valance bands are calculated with:

$$N_{\mathrm{C}} = 2\left(\frac{2\pi m_{\mathrm{e}}^{*} k_{\mathrm{B}}T}{h^2}\right)^{\frac{3}{2}} \quad (7)$$

$$N_{\mathrm{V}} = 2\left(\frac{2\pi m_{\mathrm{h}}^{*} k_{\mathrm{B}}T}{h^2}\right)^{\frac{3}{2}} \quad (8)$$

, where the necessary parameters were referred to the report. (3)

Since the refractive index change is proportional to the trapped charge carriers, $n_{\mathrm{t1}}(t)$ and $p_{\mathrm{t1}}(t)$, they reproduced the experimentally observed transient responses when $k_{\mathrm{te1}} \sim 5 \times 10^{-13}$ cm^3

s^{-1}, $k_{th1} \sim 5 \times 10^{-13}$ $cm^3 s^{-1}$. These parameters correspond for the trap depths of approximately 30 meV for both electrons and holes, which yield nanosecond-scale rise and microsecond-scale decay consistent with the PI-PM data. The model thereby explains the delayed rise of the signal as the consequence of trap filling and detrapping equilibrium at the surface.

With regard to $SrTiO_3$:Al, to reproduce the experimentally observed slower fall and recovery of the magenta (delayed-hole) response in $SrTiO_3$:Al, an additional deep hole trap state was introduced into the kinetic model described for pristine $SrTiO_3$. (**Figure S5(b)**) The governing rate equations were expressed with an additional equation for $p_{t2}(t)$ as:

For free electrons:

$$\frac{dn_m(t)}{dt} = -k_{r4} p_{t2}(t) n_m(t) - k_{te1}\left(N_{e1} - n_{t1}(t)\right) n_m(t) + k_{de1}\left(N_c - n_m(t)\right) n_{t1}(t) \quad (9)$$

For trapped electrons:

$$\frac{dn_{t1}(t)}{dt} = k_{te1}\left(N_e - n_{t1}(t)\right) n_m(t) - k_{de1}\left(N_c - n_m(t)\right) n_{t1}(t) - k_{r2} n_{t1}(t) p_m(t) \quad (10)$$

For the trapped holes at the shallow state:

$$\frac{dp_{t1}(t)}{dt} = k_{th1}\left(N_{h1} - p_{t1}(t)\right) p_m(t) - k_{dh1}\left(N_v - p_m(t)\right) p_{t1}(t) - k_{r3} p_{t1}(t) n_m(t) \quad (11)$$

For the trapped holes at the state due to Al-doping:

$$\frac{dp_{t2}(t)}{dt} = k_{th2}\left(N_{h2} - p_{t2}(t)\right) p_m(t) - k_{dh2}\left(N_v - p_m(t)\right) p_{t2}(t) - k_{r4} p_{t2}(t) n_m(t) \quad (12)$$

For free holes:

$$\frac{dp_m(t)}{dt} = \frac{dn_m(t)}{dt} + \frac{dn_{t2}(t)}{dt} - \frac{dp_{t1}(t)}{dt} - \frac{dp_{t2}(t)}{dt} \quad (13)$$

The other conditions are same as the pristine $SrTiO_3$. The kinetic scheme thus includes two hole trap levels: a shallow state ($E_{th1} \approx 50$ meV) and a newly introduced state ($E_{th2} \approx 30$ meV) associated with Al-induced defects or mixed Al–oxygen-vacancy complexes.

The simulation reproduced the slower magenta response characterized by the delayed fall and prolonged recovery observed in the experiment. The calculated transient response showed that charge accumulation occurs predominantly in the hole state during the first few microseconds, and detrapping from this state governs the long decay tail extending up to ~100 μs.

This result demonstrates that Al doping introduces a hole trap with a reduced trapping rate,

leading to the formation of long-lived trapped holes that correspond to the reactive holes identified experimentally. The simulated behavior supports the interpretation that the Al dopant modifies the valence-band structure and generates an additional metastable hole-trapping site that enhances oxidation reactivity.

For the kinetic simulation for Rh/$SrTiO_3$:Al, to reproduce the experimentally observed delayed positive (blue) response and extended electron lifetime after Rh cocatalyst loading, an additional electron-trapping cocatalyst state was incorporated into the $SrTiO_3$:Al kinetic model, as shown in **Figure S5(c)**. This new state (E_{te2}) represents the Rh cocatalyst sites that function as electron traps but do not serve as recombination center, consistent with the improved reduction reactivity observed experimentally. Thus, the kinetic model for Rh/$SrTiO_3$:Al includes two electron trap states (a shallow intrinsic state and a Rh-induced deep state) and two hole trap states (shallow and Al-induced states). The rate equations were extended with additional equation for the trapped electron state due to Rh cocatalyst as follows:

For free electrons:

$$\frac{\mathrm{d}n_{\mathrm{m}}(t)}{\mathrm{d}t} = -k_{\mathrm{r4}}p_{\mathrm{t2}}(t)n_{\mathrm{m}}(t) - k_{\mathrm{te1}}\big(N_{\mathrm{e1}} - n_{\mathrm{t1}}(t)\big)n_{\mathrm{m}}(t) + k_{\mathrm{de1}}\big(N_{\mathrm{c}} - n_{\mathrm{m}}(t)\big)n_{\mathrm{t1}}(t)$$
$$-k_{\mathrm{te2}}\big(N_{\mathrm{e2}} - n_{\mathrm{t2}}(t)\big)n_{\mathrm{m}}(t) + k_{\mathrm{de2}}\big(N_{\mathrm{c}} - n_{\mathrm{m}}(t)\big)n_{\mathrm{t2}}(t) \quad (14)$$

For the trapped electrons at the shallow state:

$$\frac{\mathrm{d}n_{\mathrm{t1}}(t)}{\mathrm{d}t} = k_{\mathrm{te1}}\big(N_{\mathrm{e1}} - n_{\mathrm{t1}}(t)\big)n_{\mathrm{m}}(t) - k_{\mathrm{de1}}\big(N_{\mathrm{c}} - n_{\mathrm{m}}(t)\big)n_{\mathrm{t1}}(t) - k_{\mathrm{r2}}n_{\mathrm{t1}}(t)p_{\mathrm{m}}(t)$$

(15)

For the trapped electrons at the state due to Rh cocatalyst:

$$\frac{\mathrm{d}n_{\mathrm{t2}}(t)}{\mathrm{d}t} = k_{\mathrm{te2}}\big(N_{\mathrm{e2}} - n_{\mathrm{t2}}(t)\big)n_{\mathrm{m}}(t) - k_{\mathrm{de2}}\big(N_{\mathrm{c}} - n_{\mathrm{m}}(t)\big)n_{\mathrm{t2}}(t)$$

(16)

For the trapped holes at the shallow state:

$$\frac{\mathrm{d}p_{\mathrm{t1}}(t)}{\mathrm{d}t} = k_{\mathrm{th2}}\big(N_{\mathrm{h2}} - p_{\mathrm{t2}}(t)\big)p_{\mathrm{m}}(t) - k_{\mathrm{dh2}}\big(N_{\mathrm{v}} - p_{\mathrm{m}}(t)\big)p_{\mathrm{t1}}(t) - k_{\mathrm{r3}}p_{\mathrm{t1}}(t)n_{\mathrm{m}}(t)$$

(17)

For the trapped holes at the state due to Al-doping:

$$\frac{\mathrm{d}p_{\mathrm{t2}}(t)}{\mathrm{d}t} = k_{\mathrm{th2}}\big(N_{\mathrm{h2}} - p_{\mathrm{t2}}(t)\big)p_{\mathrm{m}}(t) - k_{\mathrm{dh2}}\big(N_{\mathrm{v}} - p_{\mathrm{m}}(t)\big)p_{\mathrm{t2}}(t) - k_{\mathrm{r4}}p_{\mathrm{t2}}(t)n_{\mathrm{m}}(t)$$

(18)

For free holes:

$$\frac{\mathrm{d}p_{\mathrm{m}}(t)}{\mathrm{d}t} = \frac{\mathrm{d}n_{\mathrm{m}}(t)}{\mathrm{d}t} + \frac{\mathrm{d}n_{\mathrm{t1}}(t)}{\mathrm{d}t} + \frac{\mathrm{d}n_{\mathrm{t2}}(t)}{\mathrm{d}t} - \frac{\mathrm{d}p_{\mathrm{t1}}(t)}{\mathrm{d}t} - \frac{\mathrm{d}p_{\mathrm{t2}}(t)}{\mathrm{d}t} \quad (19)$$

The simulation demonstrated that electrons accumulate gradually in the Rh-induced trap state within several microseconds after excitation, forming the delayed positive component (blue) observed in the PI-PM analysis. The deeper trap depth and slower trapping rate associated with Rh sites result in extended electron lifetimes (up to ~100 μs) without significant recombination losses, explaining the experimentally observed enhancement of reduction reactivity. These results support the interpretation that Rh nanoparticles introduce electron-trapping sites that act as temporary storage centers, effectively prolonging charge separation and promoting interfacial electron-transfer processes during photocatalytic reactions.

(3) Cendula, Peter, S. David Tilley, Sixto Gimenez, et al. "Calculation of the Energy Band Diagram of a Photoelectrochemical Water Splitting Cell." *The Journal of Physical Chemistry C* 118, no. 51 (2014): 29599–607. https://doi.org/10.1021/jp509719d.

Table S1 Summary table of the parameters used in the simulation.

Material parameters, symbols	$SrTiO_3$	$SrTiO_3$:Al	Rh/$SrTiO_3$:Al
VB state density, N_v	13×10^{19} cm^{-3}	20×10^{19} cm^{-3}	20×10^{19} cm^{-3}
CB state density, N_c	7×10^{19} cm^{-3}	7×10^{19} cm^{-3}	7×10^{19} cm^{-3}
Trap state density, N_h Trap state density, N_e Trap state density by Al doping, N_{h2} Trap state density by Rh cocatalyst, N_{e2}	1×10^{17} cm^{-3} 1×10^{17} cm^{-3} --- ---	1×10^{18} cm^{-3} 1×10^{18} cm^{-3} 5×10^{17} cm^{-3} ---	1×10^{18} cm^{-3} 1×10^{18} cm^{-3} 5×10^{17} cm^{-3} 1×10^{17} cm^{-3}
Free h^+ -Trap e^- recombination, k_{r2} Free e^- -Trap h^+ recombination, k_{r3} Free e^- -Trap h^+ recombination at new state, k_{r4}	1×10^{-11} cm^3s^{-1} 1×10^{-12} cm^3s^{-1} ---	5×10^{-12} cm^3s^{-1} 5×10^{-13} cm^3s^{-1} 2×10^{-12} cm^3s^{-1}	1×10^{-13} cm^3s^{-1} 5×10^{-13} cm^3s^{-1} 3×10^{-12} cm^3s^{-1}
Hole trap at shallow state, k_{th1} Hole trap at new state, k_{th2} Electron trap at shallow state,k_{te1} Electron trap at Rh, k_{te2}	5×10^{-13} cm^3s^{-1} --- 5×10^{-13} cm^3s^{-1} ---	1×10^{-12} cm^3s^{-1} 5×10^{-15} cm^3s^{-1} 1×10^{-13} cm^3s^{-1} ---	5×10^{-13} cm^3s^{-1} 1×10^{-14} cm^3s^{-1} 1×10^{-12} cm^3s^{-1} 5×10^{-13} cm^3s^{-1}
Energy depth at shallow state, E_{th1} Energy depth at shallow state, E_{te1} Energy depth at new state, E_{th2} Energy depth at Rh, E_{te2}	30 meV 30 meV --- ---	50 meV 50 meV 30 meV ---	50 meV 50 meV 30 meV 150 meV